To be published in *Advanced Characterization Techniques for Optics, Semiconductors, and Nanotechnologies*, A. Duparré and B. Singh, Eds., Proc. SPIE **5188** (2003).

Characterizing surface roughness of thin films by polarized light scattering

Thomas A. Germer[*] and Michael J. Fasolka[†]

[*]*Optical Technology Division,* [†]*Polymers Division*
National Institute of Standards and Technology
Gaithersburg, Maryland 20899

ABSTRACT

The polarization of light scattered by the surface of a material contains information that can be used to identify the sources of that scatter. In this paper, first order vector perturbation theory for light scattering from interfacial roughness of a dielectric layer is reviewed. In addition, methods for calculating the Stokes vector for scatter from multiple sources and for decomposing a Stokes vector into contributions from two non-depolarizing scattering sources are provided. The polarization of light scattered from interfacial roughness depends upon the relative roughness of the two interfaces and the degree of phase correlation between the two interfaces. Experimental results are presented for three cases: a nominally conformal film, a nominally anticonformal film, and a lateral offset roughness film. The method works well for the nearly conformal film. Difficulties that arise for the other two cases are discussed.

Keywords: block copolymer, overlay, polarization, roughness, scattering, silicon dioxide, thin films

1. INTRODUCTION

Measurements of the polarization of scattered light can enable the distinction amongst different scattering mechanisms for the case of a single interface.[1-4] When light is directed onto a surface at an oblique angle with the electric field linearly polarized in the plane of incidence (*p*-polarized), boundary conditions force the direction of the electric field to differ on each side of the interface. The electric field just above the surface is more normal to the surface, while the electric field below the surface is more parallel to the surface. For example, in the Rayleigh approximation, a very small sphere will polarize in a direction parallel to the applied electric field and radiate as if it were an antenna in that direction. Furthermore, particles above the surface sense a field that varies in direction, amplitude, and phase with distance from the surface.[4] Scattering by small amounts of roughness behaves like a combination of the two: dipoles are induced by the electric field above the surface, and they radiate from below the surface (or vice versa).[5] For many incident-viewing geometries and incident polarizations, the scattered polarization is a signature of the scattering mechanism.[1-4]

In many cases, particle and defect detection on surfaces is hampered by the presence of surface roughness.[6] Understanding the sources of background signal enables the design of instrumentation that minimizes the signal from such sources. Since the polarization from single interface micro-roughness is defined by the geometry and the optical constants of the material and not the roughness function, a device that collects light over most of the hemisphere, yet is blind to micro-roughness, can be built.[7] Such a device can substantially improve the sensitivity for detecting particles and defects on rough surfaces. However, successful application of this technique for the inspection of materials with dielectric layers requires knowledge of the polarization of scattering from different sources, including interfacial roughness.[4]

Previous work on single interfaces raises questions about whether polarized light scattering techniques can be applied to characterize roughness in dielectric multilayers.[1] Such layers are interesting technologically, as they are found ubiquitously in optics, microelectronics, data storage media, and information display systems. In this manuscript, we review the theory for light scattering from micro-roughness of the interfaces of a single dielectric layer and explore an application of that theory. Next, we discuss the scattering from two sources (i.e. roughness of each of two interfaces) and describe how polarized light scattering enables quantification of the morphology of these two different scattering sources. Finally, this theory is applied to experimental data from three different samples, the interfacial topography of which was chosen to challenge the limits of the method.

In Sec. 2, we describe a theoretical treatment for scattering from rough surfaces. Included in Sec. 2 is a method for treating multiple sources that maintains all the polarimetric information, and a method for decomposing a measured polarization state into the sum of two different non-depolarizing scattering sources. In Sec. 3, we apply the theory to a specific system consisting of a 52 nm SiO_2 layer grown on silicon, and we compare the model calculations to experimental data. Finally, in Sec.4 the work is summarized and conclusions will be drawn.

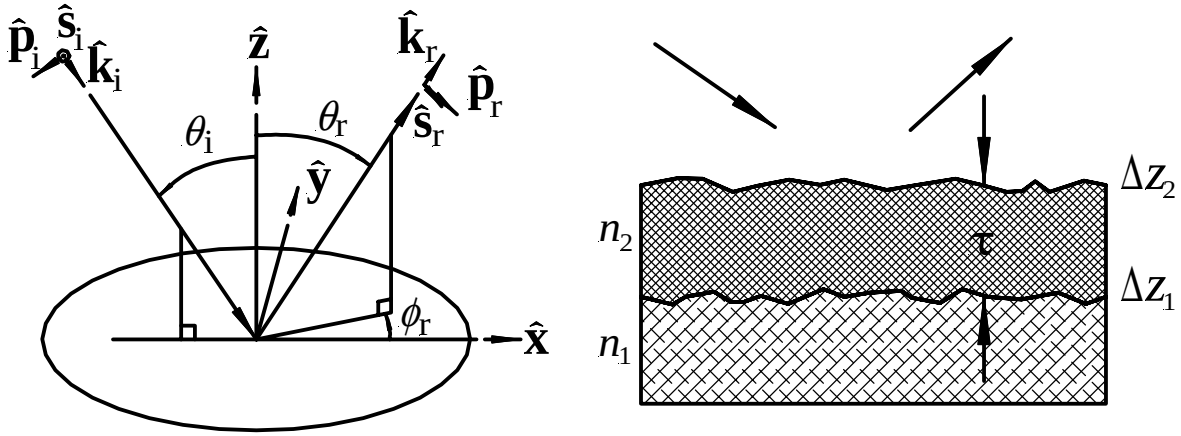

Figure 1. (left) Schematic diagram showing the global scattering geometry and the various angles and vectors discussed in the text. (right) Schematic diagram showing a thin film with rough interfaces.

2. THEORY

2.1. General considerations

Figure 1 shows schematic diagrams of the scattering geometry and the sample topography. Here, plane wave polarized light of wavelength λ irradiates the surface at an incident angle θ_i in the plane defined by unit vectors $\hat{\mathbf{x}}$ and $\hat{\mathbf{z}}$. We are interested in determining the Jones or Mueller matrix for scattering into a direction defined by a polar angle θ_r and an azimuthal (out-of-plane) angle ϕ_r. Unit vectors $\hat{\mathbf{k}}_i$ and $\hat{\mathbf{k}}_r$ describe the propagation-directions of the incident and scattered light, respectively. The polarization of the incident electric field is described by the components of the electric field along the $\hat{\mathbf{s}}_i$ and $\hat{\mathbf{p}}_i$ directions, where $\hat{\mathbf{s}}_i$ is a unit vector perpendicular to both $\hat{\mathbf{k}}_i$ and $\hat{\mathbf{z}}$, and $\hat{\mathbf{p}}_i = \hat{\mathbf{k}}_i \times \hat{\mathbf{s}}_i$. Likewise, the polarization of the electric field scattered into a particular direction is described by components along the $\hat{\mathbf{s}}_r$ and $\hat{\mathbf{p}}_r$ unit vectors, defined in an analogous manner as $\hat{\mathbf{s}}_i$ and $\hat{\mathbf{p}}_i$. We say that light is *p*-polarized (*s*-polarized) when it is polarized with its electric field parallel to $\hat{\mathbf{p}}$ ($\hat{\mathbf{s}}$). Throughout this discussion, we omit the $\exp(-i\omega t)$ time dependence for all fields.

The scattering (Jones) matrix $\mathbf{S}$ is defined as the relationship between the incident and scattered fields:

$$\begin{pmatrix} E_s^{scat} \\ E_p^{scat} \end{pmatrix} = \frac{\exp(ikR)}{R} \begin{pmatrix} S_{ss} & S_{ps} \\ S_{sp} & S_{pp} \end{pmatrix} \begin{pmatrix} E_s^{inc} \\ E_p^{inc} \end{pmatrix}, \tag{1}$$

where *R* is the distance between the scattering source to the detector, and $k = 2\pi/\lambda$. The intensity relationship can be expressed using the Stokes-Mueller representation, via the bidirectional reflectance distribution function (BRDF) $\mathbf{F}_r$,

$$d\mathbf{\Phi}_r = \mathbf{F}_r \, \mathbf{\Phi}_i \cos\theta_r \, d\Omega, \tag{2}$$

where $\mathbf{\Phi}_i$ is the incident Stokes power vector, $d\mathbf{\Phi}_r$ is the differential scattered Stokes power vector, and $d\Omega$ is the differential solid angle. The $\cos\theta_r$ factor is customary in the definition of the BRDF.[6,8] The Mueller matrix $\mathbf{F}_r$ can be derived from the Jones matrix **S** using

$$\mathbf{F}_\mathrm{r} = \mathbf{M}(\mathbf{S})/(A\cos\theta_\mathrm{i}\cos\theta_\mathrm{r}), \tag{3}$$

where A is the illuminated area on the sample and $\mathbf{M}(\mathbf{S})$ represents the Jones to Mueller transformation found in numerous places in the literature.[9-11]

A Stokes vector power, $\mathbf{\Phi}$, is characterized by each of its elements Φ_j (j = 0,1,2,3). For our application, it is convenient to signify the polarization state through the principal angle of the polarization ellipse, η, and various degrees of polarization. The principal angle η is given by

$$\eta = \arctan(\Phi_1, \Phi_2)/2, \tag{4}$$

where the two argument $\arctan(a,b)$ takes into account in which quadrant the point (a,b) lies. The angle η is measured counterclockwise from $\hat{\mathbf{s}}$, along the incident direction. The total degree of polarization is

$$P = (\Phi_1^{\,2} + \Phi_2^{\,2} + \Phi_3^{\,2})^{1/2}/\Phi_0, \tag{5}$$

and the degree of circular polarization is

$$P_\mathrm{C} = \Phi_3/\Phi_0. \tag{6}$$

Depolarization (P < 1) results from a polarization state that varies, either in time or in space. The parameters Φ_0, η, P_C, and P completely describe the polarization and intensity of the light. The use of these parameters over the Stokes parameters follows from the work on single interfaces. In such cases, P = 1 and P_C = 0, so that η serves to indicate the scattering mechanism. However, it should be noted that these parameters do not behave linearly, and uncertainties scale with respect to their magnitude. For example, when P_C = 1 or –1, the value of η is not well-defined.

In the following subsections, we consider scattering from interfacial micro-roughness (Sec. 2.2.). In particular, we will present formalisms for summing two scattering sources and for decomposing a Stokes vector into the amplitudes and correlation function of two scattering sources (Sec. 2.3.).

2.2. First order vector perturbation theory

Figure 1 (right) shows a cross section of the dielectric film and defines the indices of refraction n_1 and n_2, the thickness τ, and the surface height functions Δz_1 and Δz_2. Generally, first-order vector perturbation theory successfully describes the intensity and polarization of light scattered by small amounts of roughness.[12] In this model, zero-order ("unperturbed", Δz_1 = 0 and Δz_2 = 0) fields are determined from the standard analysis of reflection from a dielectric film. The calculation consists of a first-order expansion of both the electric and magnetic fields on both sides of each interface of the local surface normal in the surface height function, $\Delta z_m(x,y)$, about its mean. The requirement that the tangential electric and magnetic fields be continuous across the boundary leads to relationships between zero-order and first-order fields. Given this, the theory self-consistently handles the multiple reflections that occur for both orders of the field. However, since this model assumes that the film thickness is constant, it does not account for long-range non-conformal roughness, which can exhibit substantial variation in local film thickness. Accordingly, in order for the theory to be valid, modulations of the surface height functions, $\Delta z_m(x,y)$, must be much less than the wavelength, λ, and the surface slope must be much less than unity.

Elson described the solution to first-order vector perturbation theory for scattering from interfacial micro-roughness in a dielectric stack.[12-16] Since Ref. 12 thoroughly describes this calculation, we will not repeat it here. However, for our discussion it is useful to present the less general solutions for roughness of each interface of a single dielectric overlayer (three-phase model), which can be simplified considerably. For the buried interface (1), the scattering matrix elements are given by

$$S_{uv}^{(1)} = (4/\pi)(n_1^{\,2} - n_2^{\,2})\exp[\mathrm{i}(q_{\mathrm{i}2} + q_{\mathrm{r}2} - q_{\mathrm{r}3} - q_{\mathrm{i}3})\tau]q_{\mathrm{r}3}q_{\mathrm{i}3}A^{1/2}\Delta Z_1(\mathbf{q})s_{uv}^{(1)}, \tag{7}$$

(u, v = s, p) where

$$s_{\rm pp}^{(1)} = -n_2^{\,2} q_{\rm i2} q_{\rm r2} (n_1^{\,2} k_{\rm i} k_{\rm r} - n_2^{\,2} q_{\rm i1} q_{\rm r1} \cos\phi_{\rm r}) / (\Gamma_{\rm pi} \Gamma_{\rm pr}), \tag{8a}$$

$$s_{\rm ps}^{(1)} = n_2^{\,2} k q_{\rm i2} q_{\rm r2} q_{\rm i1} \sin\phi_{\rm r} / (\Gamma_{\rm pi} \Gamma_{\rm sr}), \tag{8b}$$

$$s_{\rm sp}^{(1)} = n_2^{\,2} k q_{\rm i2} q_{\rm r2} q_{\rm r1} \sin\phi_{\rm r} / (\Gamma_{\rm si} \Gamma_{\rm pr}), \tag{8c}$$

$$s_{\rm ss}^{(1)} = -k^2 q_{\rm i2} q_{\rm r2} \cos\phi_{\rm r} / (\Gamma_{\rm si} \Gamma_{\rm sr}), \tag{8d}$$

$$\Gamma_{{\rm p}\beta} = n_2^{\,2} F_{{\rm p}\beta}^{(+)} q_{\beta 3} - F_{{\rm p}\beta}^{(-)} q_{\beta 2}\,, \tag{9a}$$

$$\Gamma_{{\rm s}\beta} = F_{{\rm s}\beta}^{(+)} q_{\beta 3} - F_{{\rm s}\beta}^{(-)} q_{\beta 2}\,, \tag{9b}$$

$$F_{{\rm p}\beta}^{(\pm)} = n_2^{\,2} K_\beta^{(\mp)} q_{\beta 1} - n_1^{\,2} K_\beta^{(\pm)} q_{\beta 2}, \tag{10a}$$

$$F_{{\rm s}\beta}^{(\pm)} = K_\beta^{(\mp)} q_{\beta 1} - K_\beta^{(\pm)} q_{\beta 2}, \tag{10b}$$

$$K_\beta^{(\pm)} = \exp(2{\rm i} q_{\beta 2} \tau) \pm 1, \tag{11}$$

$q_{\beta j} = k(n_j^{\,2} - \sin^2\theta_\beta)^{1/2}$, and $k_\beta = k \sin\theta_\beta$ (β = i or r and j = 1 or 2). The Fourier transform of the roughness of the m-th interface is given by

$$\Delta Z_m(\mathbf{q}) = A^{-1/2} \int_A {\rm d}^2\mathbf{r}\; \Delta z_m(\mathbf{r}) \exp[{\rm i}\mathbf{q}\cdot\mathbf{r}]\,, \tag{12}$$

where $\Delta z_m(\mathbf{r})$ is the surface height function of the m-th layer about its mean value, and the integration is carried out over the irradiated area A. The power spectral density (PSD) function is $\left\langle \left| \Delta Z_m(\mathbf{q}) \right|^2 \right\rangle$, averaged over an ensemble of realizations. The vector $\mathbf{q}$ is the 2-d surface wavevector, related to the scattering directions by

$$q_x = k_{\rm r} \cos\phi_{\rm r} - k_{\rm i}, \tag{13a}$$

$$q_y = k_{\rm r} \sin\phi_{\rm r}\,. \tag{13b}$$

For the exposed interface (2), the scattering matrix elements are given by

$$S_{uv}^{(2)} = (1/\pi)(n_2^{\,2} - 1) q_{\rm r3} q_{\rm i3} \exp[{\rm i}(-q_{\rm i3} - q_{\rm r3})\tau] A^{1/2} \Delta Z_2(\mathbf{q}) s_{uv}^{(2)}, \tag{14}$$

where

$$s_{\rm pp}^{(2)} = -(n_2^{\,2} k_{\rm i} k_{\rm r} F_{\rm pi}^{(+)} F_{\rm pr}^{(+)} - q_{\rm i2} q_{\rm r2} F_{\rm pi}^{(-)} F_{\rm pr}^{(-)} \cos\phi_{\rm r}) / (\Gamma_{\rm pi} \Gamma_{\rm pr}), \tag{15a}$$

$$s_{\rm ps}^{(2)} = -k q_{\rm i2} F_{\rm pi}^{(-)} F_{\rm sr}^{(+)} \sin\phi_{\rm r} / (\Gamma_{\rm pi} \Gamma_{\rm sr}), \tag{15b}$$

$$s_{\rm sp}^{(2)} = -k q_{\rm r2} F_{\rm si}^{(+)} F_{\rm pr}^{(-)} \sin\phi_{\rm r} / (\Gamma_{\rm si} \Gamma_{\rm pr}), \tag{15c}$$

$$s_{\rm ss}^{(2)} = -k^2 F_{\rm si}^{(+)} F_{\rm sr}^{(+)} \cos\phi_{\rm r} / (\Gamma_{\rm si} \Gamma_{\rm sr}). \tag{15d}$$

The scattering matrix elements in Eqs. (7) and (14) depend upon the surface height functions of the respective interfaces, but only as a common multiplicative product. That is, the surface-height functions affect the intensity, but not the polarization of the scattered light. Therefore, to first order, the scattering from a single rough interface will not depolarize light. Furthermore, the fields resulting from the scattering of each interface are independent of each other. An implementation of the theory described in this section is found in the SCATMECH C++ scattering code library,[17] as TWO_FACE_BRDF_MODEL.

2.3. Decomposition of a Stokes vector into contributions from two non-depolarizing sources

Suppose that we have two, and only two, sources of light, that we can calculate the Jones vectors, $\mathbf{J}_1$ and $\mathbf{J}_2$, resulting from each source, and that they are independent. The sum of the two Jones vectors can be written as

$$\mathbf{J}_{\text{tot}} = \kappa_1 \mathbf{J}_1 + \kappa_2 \mathbf{J}_2 \tag{16}$$

where κ_1 and κ_2 are complex scaling factors and are random variables. To lowest order in the surface height function, micro-roughness of two interfaces of a dielectric film satisfies these requirements, and a prescription for determining $\mathbf{J}_1$ and $\mathbf{J}_2$ is found in Sec. 2.2. That is, in the case of thin film micro-roughness, $\mathbf{J}_1$ and $\mathbf{J}_2$ can be written so that $\kappa_1 = \Delta Z_1$ and $\kappa_2 = \Delta Z_2$. After some algebra, the mean Stokes vector is given by

$$\begin{aligned} S_{\text{tot},0} = {} & \left\langle |\kappa_1|^2 \right\rangle \left(|J_{1s}|^2 + |J_{1p}|^2 \right) + \left\langle |\kappa_2|^2 \right\rangle \left(|J_{2s}|^2 + |J_{2p}|^2 \right) + \\ & \operatorname{Re}\left\langle \kappa_1 \kappa_2^* \right\rangle \left(2 \operatorname{Re} J_{2s} J_{1s}^* + 2 \operatorname{Re} J_{2p} J_{1p}^* \right) + \operatorname{Im}\left\langle \kappa_1 \kappa_2^* \right\rangle \left(2 \operatorname{Im} J_{2s} J_{1s}^* + 2 \operatorname{Im} J_{2p} J_{1p}^* \right) \end{aligned} \tag{17a}$$

$$\begin{aligned} S_{\text{tot},1} = {} & \left\langle |\kappa_1|^2 \right\rangle \left(|J_{1s}|^2 - |J_{1p}|^2 \right) + \left\langle |\kappa_2|^2 \right\rangle \left(|J_{2s}|^2 - |J_{2p}|^2 \right) + \\ & \operatorname{Re}\left\langle \kappa_1 \kappa_2^* \right\rangle \left(2 \operatorname{Re} J_{2s} J_{1s}^* - 2 \operatorname{Re} J_{2p} J_{1p}^* \right) + \operatorname{Im}\left\langle \kappa_1 \kappa_2^* \right\rangle \left(2 \operatorname{Im} J_{2s} J_{1s}^* - 2 \operatorname{Im} J_{2p} J_{1p}^* \right) \end{aligned} \tag{17b}$$

$$\begin{aligned} S_{\text{tot},2} = {} & \left\langle |\kappa_1|^2 \right\rangle \left(2 \operatorname{Re} J_{1p} J_{1s}^* \right) + \left\langle |\kappa_2|^2 \right\rangle \left(2 \operatorname{Re} J_{2p} J_{2s}^* \right) + \\ & \operatorname{Re}\left\langle \kappa_1 \kappa_2^* \right\rangle \left(2 \operatorname{Re} J_{2p} J_{1s}^* + 2 \operatorname{Re} J_{2s} J_{1p}^* \right) + \operatorname{Im}\left\langle \kappa_1 \kappa_2^* \right\rangle \left(2 \operatorname{Im} J_{2p} J_{1s}^* + 2 \operatorname{Im} J_{2s} J_{1p}^* \right) \end{aligned} \tag{17c}$$

$$\begin{aligned} S_{\text{tot},3} = {} & \left\langle |\kappa_1|^2 \right\rangle \left(2 \operatorname{Im} J_{1p} J_{1s}^* \right) + \left\langle |\kappa_2|^2 \right\rangle \left(2 \operatorname{Im} J_{2p} J_{2s}^* \right) + \\ & \operatorname{Re}\left\langle \kappa_1 \kappa_2^* \right\rangle \left(2 \operatorname{Im} J_{1p} J_{2s}^* - 2 \operatorname{Im} J_{1s} J_{2p}^* \right) + \operatorname{Im}\left\langle \kappa_1 \kappa_2^* \right\rangle \left(2 \operatorname{Re} J_{1p} J_{2s}^* - 2 \operatorname{Re} J_{1s} J_{2p}^* \right) \end{aligned} \tag{17d}$$

If $\mathbf{J}_1$ and $\mathbf{J}_2$ are linearly independent (that is, $\mathbf{J}_1 \cdot \mathbf{J}_2^* \neq 0$), Eq. (17) can be solved for $\left\langle |\kappa_1|^2 \right\rangle$, $\left\langle |\kappa_2|^2 \right\rangle$, $\operatorname{Re}\left\langle \kappa_1 \kappa_2^* \right\rangle$, and $\operatorname{Im}\left\langle \kappa_1 \kappa_2^* \right\rangle$. We define a relative scaling factor

$$\chi = \left(\left\langle |\kappa_2|^2 \right\rangle \Big/ \left\langle |\kappa_1|^2 \right\rangle \right)^{1/2}$$

and a phase correlation function

$$C_{12} = \left\langle \kappa_1 \kappa_2^* \right\rangle \Big/ \left(\left\langle |\kappa_1|^2 \right\rangle \left\langle |\kappa_2|^2 \right\rangle \right)^{1/2}.$$

The parameters χ and C_{12} determine the polarization state of the scattered light, while $\left\langle |\kappa_1|^2 \right\rangle$ or $\left\langle |\kappa_2|^2 \right\rangle$ determine the intensity. By applying Eq. (17), we can readily calculate the Stokes vector BRDF for scattering from the surfaces of a dielectric film. Indeed, this approach can be applied to a wide range of surface relationships including correlated roughness ($C_{12} = 1$), uncorrelated ($C_{12} = 0$) and partially correlated ($0 < |C_{12}| < 1$) roughness, or even anti-correlated ($C_{12} = -1$) film surfaces. Cases of equal ($\chi = 1$) and unequal ($\chi \neq 1$) roughness amplitudes can also be considered. Likewise, given a measured Stokes vector, we can determine χ and C_{12}.

3. EXPERIMENT

Measurements were performed using the Goniometric Optical Scatter Instrument (GOSI) at NIST.[18,19] GOSI is a laser-based angle-resolved scattering system having a high angular resolution, wide dynamic range, full polarimetric capability, and the ability to measure scattering out of the plane of incidence. Measurements performed for this study by

GOSI used either a HeNe laser (λ = 632.8 nm) or a doubled Nd:YAG laser (λ = 532 nm). Measurement geometries involved either a fixed incident angle θ_i while scanning the scattering angle θ_r in the plane of incidence, or a fixed incident and scattering angle ($\theta_r = \theta_i$), while scanning ϕ_r out of the plane of incidence. The instrument is capable of full Mueller matrix measurements. However, only measurements of the Stokes vector were performed, using 45° incident polarization for in plane measurements, or using a varying incident polarization state $\eta_i = 45° + \phi_r/2$ for the out-of-plane measurements. Both incident polarization schemes yield a high degree of discrimination between scattering sources. The intensity and polarization of the scattered light is characterized by the polarization-averaged bidirectional reflectance distribution function (BRDF), f_r, the principal angle of the polarization, η (measured counterclockwise from s-polarization when looking into the direction of propagation), the degree of circular polarization, P_C, and the total degree of polarization, P.

A full uncertainty analysis has not been completed for these measurements. However, experience shows that the uncertainties are dominated by statistical noise in the data, which arises from both electronic noise and from speckle noise; these can be estimated by apparent point-to-point fluctuations in the data. Systematic uncertainties are typically much less than these fluctuations.

4. EXAMPLES

In this section we describe measurements on three fabricated model film systems, schematically illustrated in Fig. 2. These specimens represent extremes that delineate the utility of light scattering for measuring surface roughness. In Secs. 4.1, 4.2, and 4.3, respectively, we discuss measurements on:

- a nearly *conformal* SiO_2 layer grown on topographically structured silicon substrate,
- an *anticonformal* block copolymer film deposited on a silicon substrate identical to that of the first case,
- a sample fabricated to have a low profile pattern on one interface, and an identical, but *laterally offset*, pattern on the other interface.

While the first (conformal) specimen illustrates a case where our analysis approach worked very well, the second two samples present significant challenges to the method.

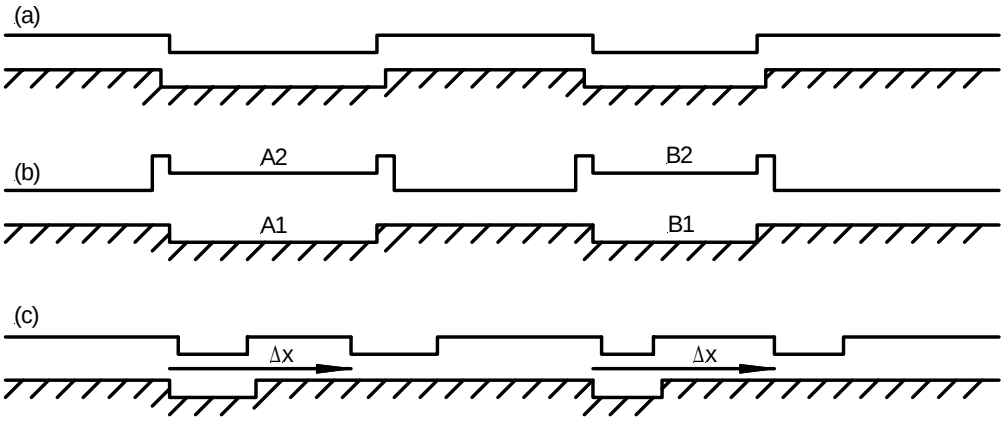

Figure 2. Schematic of the three samples: (a) the conformal SiO_2 layer on silicon, (b) the anticonformal PS-POMA diblock copolymer on silicon, and (c) the lateral offset pattern. The labels in (b) refer to the discussion in the text. The arrows in (c) indicate the lateral offset distance, Δx.

4.1. Nearly conformal roughness

The first sample consisted of a 52 nm SiO_2 film thermally grown on a photolithographically-produced micro-rough silicon surface. The micro-rough substrate consisted of a pseudorandom distribution of shallow circular pits (8 nm deep) having nominal diameters of 1.31 µm and 1.76 µm.[20] This system was intended to exhibit conformal roughness, at least for small spatial frequencies. Fig. 2(a) shows a schematic cross-section of this system.

Measurements were performed in the out-of-plane configuration with $\theta_i = \theta_r = 68°$, using the variable incident polarization scheme and $\lambda = 532$ nm. The results of these measurements are shown in Fig. 3 on the left. Included with the scattering polarimetric data are calculated curves corresponding to four conditions: equal and correlated roughness, equal but uncorrelated roughness, and roughness of each of the two interfaces alone. As illustrated by comparing the data to the model curves, at small angles ($\phi_r < 15°$), the system behaves like the equal roughness case, but at larger scattering angles the results deviate significantly from this model. Using the method outlined in Sec. 2.3, the roughness PSD of each interface, the relative roughness of the two interfaces, and the degree of correlation were determined from the data.[21] Figure 3 shows the results of this analysis. The indicated uncertainties represent single standard deviations of the extracted results propagated from the spread in several measurements made at each point. These uncertainties do not represent all of the systematic sources of uncertainty that might exist. The results show that $\chi > 1$ and $C_{12} \sim 1$ for most spatial frequencies, consistent with the smoothening of the growth (i.e. buried) interface. Further validation of the method was achieved by performing the measurements at multiple wavelengths and incident angles.[21]

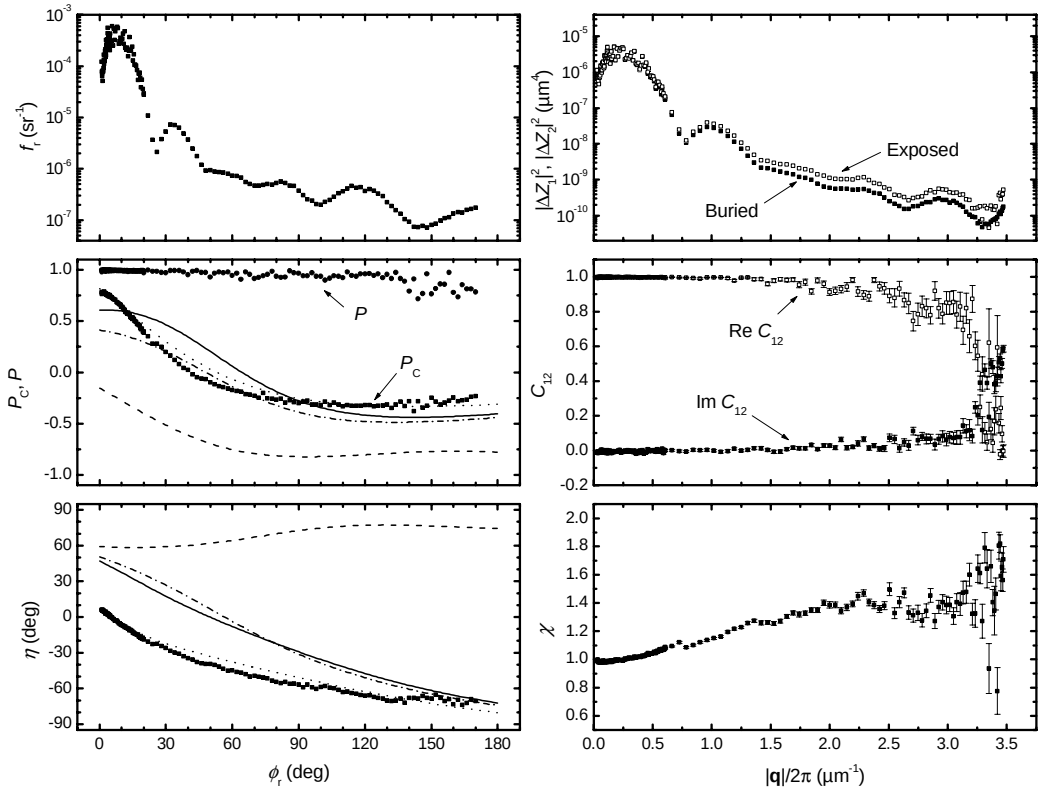

Figure 3. Results of measurements and analysis on the approximately conformal SiO_2 layer on silicon. The curves show the theoretical predictions for (solid) buried interface roughness, (long dash) exposed interface roughness, (short dash) equal and correlated roughness, and (dash dot) equal but uncorrelated roughness.

In addition to the smoothening of the buried interface, another feature was observed in the extracted results. There is a small, yet reproducible, feature in χ at a spatial frequency of about 0.7 μm^{-1}. This wiggle, which corresponds to a relative roughness change of less than 4 %, results from the buried interface pits being slightly larger than the corresponding exposed interface pit (see Fig. 2). The power spectrum of circular pits of diameter D, depth t, and surface density ρ, is given by

$$\left\langle \left|\Delta Z(q)\right|^2 \right\rangle = \rho[tD\,\mathrm{J}_1(qD/2)/(2q)]^2 . \tag{18}$$

A change in the width of a pit relative to the corresponding feature on the other interface causes the spatial frequencies at which the surface roughness is zero to shift, resulting in the derivative-like feature. A similar feature can be observed near a spatial frequency of 2.7 μm^{-1} in the two power spectra. The local minimum occurs at slightly different spatial

frequencies. These results are entirely consistent with the isotropic growth of SiO_2 on silicon. Indeed, these findings are a testament to the sensitivity that the technique has to measuring small changes in relative surface roughness.

4.2. Anticonformal roughness

An interesting case of thin film surface roughness is the case of anticonformal roughness, where the exposed surface undulates exactly out of phase with the buried interface. For this study, we fabricated an anticonformal system on a pitted SiO_2 substrate (as in Sec. 4.1) using diblock copolymers, which consist of two polymer chains (blocks) covalently bound at one end. If the constituent chains are immiscible, diblock copolymers self assemble into nano-metric domains with a regular periodicity, L; volume-symmetric species exhibit a lamellar motif. In thin films, preferential wetting of one or the other block at the film interfaces generally results in surface-parallel layered structures.[22] For symmetric wetting systems (same block found at the substrate and free surface), stable conformal films are formed when the film thickness accommodates an integral number of microdomain periods. When the film thickness (h) is incommensurate with L, the free surface of the film bifurcates into relief structures that are L in height. The amount and morphology of this "incomplete" layer depends upon the magnitude of the mismatch between h and the closest stable film condition ($h=mL$, with m an integer). We harness these surface relief structures to form an anticonformal film. Here, h is chosen such that $(h–mL)/mL$ equals the fractional area of pits on the substrate (≈15%). This, in conjunction with the fact that the pits nucleate surface relief structures,[23] results in the formation of round islands that sit over the pits and that have diameters roughly equal to the underlying pits – an anticonformal film. Our anticonformal specimen was realized using a volume symmetric Polystyrene-b-Polyoctylmethacrylate (PS-b-POMA) diblock copolymer with relative molecular mass M_r = 47K Daltons and L = 23 nm. While the indices are slightly different [n_{PS} = 1.59 versus n_{POMA}=1.48], they are sufficiently close to ignore in this study. In films on SiO_2, POMA resides at both the exposed and substrate interfaces, resulting in surface-parallel lamellae with the following structure:

$$SiO_2 \mid POMA – PS \mid PS – POMA \mid ... \mid POMA – PS \mid PS – POMA \mid Air$$

Thin films of PS-b-POMA were deposited from toluene solution onto pitted substrates via spin-casting. Adjustment of the spin-speed enabled films that were approximately 2.15L thick. Annealing at 130 °C for 2 hours induced self-assembly and the formation of anticonformal structures, as verified by atomic force microscopy (AFM). The film thickness over most of the sample was 46 nm (2L), while that above the pits was 69 nm (3L). A schematic of the nominal sample is shown in Fig. 2(b). As shown in this diagram, there is a small amount of material spillover (in the lateral direction) around the pits about 170 nm wide.

Measurements were performed in the out-of-plane configuration with $\theta_i = \theta_r = 60°$, using the variable incident polarization scheme and λ = 532 nm. The results are shown in Fig. 4 on the left. The data shows significantly more structure than that observed in Fig. 3. For example, there are dips in the degree of polarization at angles where there is structure in the intensity. Figure 4 also shows the roughness PSD of each interface, the relative roughness of the two interfaces, and the degree of correlation extracted from the data using the method outlined in Sec. 2.3. Using the nominal dimensions given above, and using the power spectrum given in Eq. (18), we estimate these parameters, which are included in Fig. 4. In making the estimates, we increased the dimension of all radii by 0.1 µm, so that the locations of features better matched those seen in the experimental results.

Agreement between the experimentally determined surface statistics and that predicted by the simple model is very good in certain respects. The modeled relative roughness, χ, and the correlation function exhibit oscillations with magnitudes similar to those of the observed data. The calculated and measured power spectra of the surfaces behave similarly, although there is a large offset between the model and the data. These similarities allow us to make conclusions about the origin of features that are well reproduced by the model. The basic correspondence of the shape of the power spectral densities suggests that our model reasonably approximates the surface topography. The reduction of correlation between the two surfaces (for example, at 0.6 μm^{-1} and 1.1 μm^{-1}) results from the significant spillover of the exposed surface features. When viewing the surface at a spatial frequency where one specific pit or mound yields a vanishing power spectral density [see Eq. (18)], the power spectral density of the corresponding feature above or below it is far from vanishing. For example, at spatial frequencies where the scattering by feature A1 in Fig. 2 vanishes, the scattering by feature A2 does not. However, feature A2 lacks any correlation with feature B1. Therefore, when the scattering from feature A1 vanishes, there will be a partial lack of correlation between the top and bottom interfaces. This lack of correlation between the interfaces exists despite the deterministic nature of the surface topography. At

spatial frequencies higher than those modeled (about 1.4 μm^{-1}), correlation is expected to diminish, as is observed in Fig. 4, since there is likely significant variation in the spillover distance.

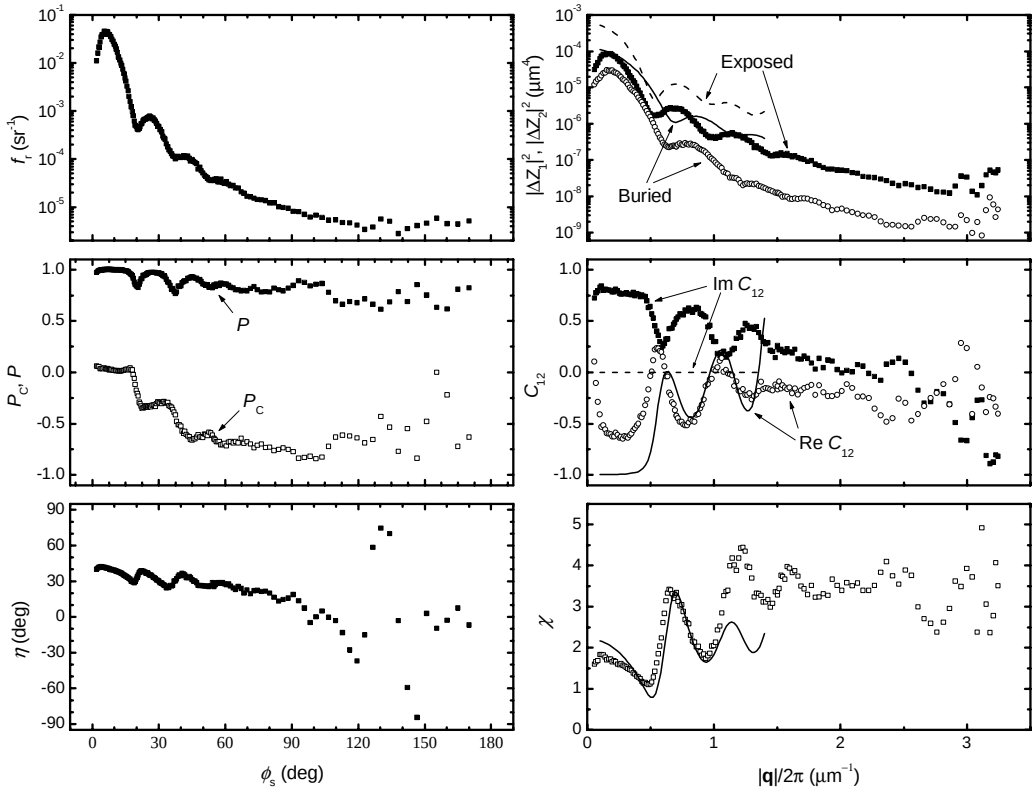

Figure 4. Results of measurements and analysis on the approximately anticonformal diblock copolymer layer on silicon. The curves shown with the derived surface statistics are those predicted by the surface model described in the text.

In other aspects, agreement between the experimentally determined surface statistics and that predicted by the simple model are comparatively poor. Most troubling is the disagreement observed in the phase of the correlation parameter C_{12}, which the model predicts should be real. This phase results from the significant vertical height of the surface topography, which results in significant variation of the film thickness. The total change of the film thickness above the pits of the silicon interface is approximately 23 nm, which is large in ellipsometric terms. That is, the phase resulting from this height difference is substantial enough that it cannot be accommodated by the simple theory. An estimate of the phase change that would occur due to such a change in the film thickness, given the index of the layer, the wavelength, and the incident and scattering angles, is approximately 60°, close to that observed at low spatial frequencies. That is, the modulation of the thickness of the material is too great to apply first-order perturbation theory. Unfortunately, higher order scattering is much more difficult to interpret, since the scattered field is no longer proportional to the Fourier transform of the surface height function.

4.3. Laterally Offset Roughness

Another interesting case of roughness statistics is that of laterally offset roughness. In this case, a pattern is identical (at least nominally) on the two surfaces, but is offset by a distance $\Delta\mathbf{x}$. The phase correlation function would then be

$$C_{12} = \exp(i\mathbf{q}\cdot\Delta\mathbf{x}) . \tag{19}$$

In order to produce a sample with this characteristic, we first lithographically etched a silicon substrate with parallel lines, approximately 29 nm deep, and having nominal widths varying from 1.5 µm to 5.2 µm with a pseudorandom spacing. Next, the patterned specimen was thermally oxidized to a depth of about 270 nm. Finally, a second

lithography step was used to produce a 20 nm deep pattern in the top interface. The second lithography step was performed using the same mask used to create the first pattern, except that an intentional 50 μm offset was imposed in a direction perpendicular to the lines. Because of the nearly conformal growth of the thermal oxide, the top surface contains features associated with both lithography steps. A schematic of the sample is shown in Fig. 2(c).

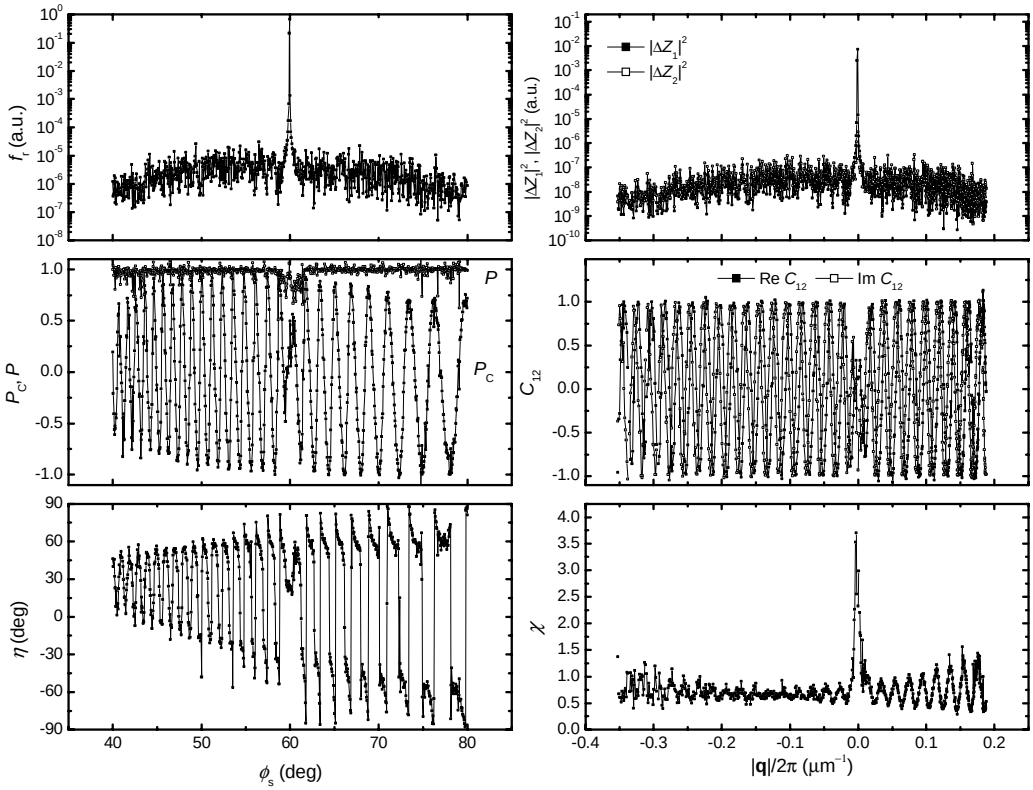

Figure 5. Results of measurements and analysis on the laterally offset roughness layer on silicon. The intensity and power spectrum results are shown with arbitrary units, since an absolute measurement of the incident intensity was not performed. The lines connect the data points and are intended to guide the reader's eye.

Data were collected in the plane of incidence using 45° incident polarization and 633 nm light using a 0.02° slit collection aperture. Figure 5 shows the measured data along with the calculated surface statistics. Despite a relatively featureless intensity profile, the polarization state of the light oscillates between nearly orthogonal states. Extraction of the surface statistics from the measured data was accomplished assuming that the film thickness was 270 nm and that the pattern on the buried interface is replicated on the exposed interface. That is, the two sources used in the analysis were

$$\mathbf{J}_1 = \mathbf{J}_e + \mathbf{J}_b \tag{20a}$$

$$\mathbf{J}_2 = \mathbf{J}_e \tag{20b}$$

where $\mathbf{J}_e$ is the Jones vector calculated for the exposed interface, using Eq. (14), and $\mathbf{J}_b$ is the Jones vector calculated for the buried interface, using Eq. (7). The correlation function shows periodic oscillations, as predicted by Eq. (19). Indeed, a fit to Eq. (19) yields $\Delta\mathbf{x}$ = 49.45 μm, with a standard uncertainty of about 0.03 μm, in good agreement with the nominal offset of 50 μm.

However, there are inconsistencies in the data that warrant discussion as they likely reduce the accuracy of the method as a means for overlay metrology. For example, Fig. 5 also shows oscillations in χ, which are not predicted by the model. The value of χ in the region where the oscillation amplitude is a minimum, about χ = 0.7, is roughly that expected from our knowledge of the pit depths (20 nm/29 nm). These oscillations may be a result of the imperfect

replication of the buried interface onto the exposed interface. As discovered in Sec. 4.1, the oxide growth process does not provide an identical replication of the interfaces, so Eq. (20a) is not completely correct. While we do not have sufficient information under these growth conditions to completely rule out replication effects, the asymmetry in the oscillations in χ suggest that the replication function is not the sole source of this problem. It also may be that the film thickness used in the calculations is incorrect. Indeed, changing the mean film thickness from 270 nm to 285 nm yields a more symmetric χ function. However, this solution to the problem cannot be correct, since using the thicker value and changing the balance between the two Jones vectors in Eq. (20a) does not remove the oscillations in a consistent manner.

It is most likely that the problem in interpreting the data in Fig. 5 is similar to that found for the anticonformal film described in Sec. 4.2. That is, the modulation of the thickness of the material is too great to apply first-order perturbation theory. The thickness of the film around the conformal features remains relatively constant. However, the features etched into the exposed interface reduce the thickness of the film by about 20 nm. The optical phase introduced by this large height modulation is not treated by the theory.

5. SUMMARY AND CONCLUSIONS

In this paper, we reviewed models for polarized light scattering from interfacial roughness. In addition, we outlined a method by which polarized light scattering measurements can be used to determine the roughness of the two interfaces of a dielectric film. While the method worked very well for a conformal film, it suffered from some problems when the analysis was extended to anticorrelated and overlay roughness. It is believed that the breakdown of the analysis results from the use of first order perturbation theory in conditions where the thickness of the film varied substantially. These issues suggest that the limits on first order vector perturbation theory for thin films is significantly tighter than those imposed for single interfaces. It is expected, however, that the methods described in this paper would be suitable for characterizing naturally occurring thin films, which most often exhibit gentler topographic features.

ACKNOWLEDGEMENTS

The authors thank Brad Scheer, formerly of VLSI Standards, Inc., for providing the conformal oxide sample, Anne M. Mayes, Dept. of Materials Science and Engineering, MIT, for supplying the PS-POMA diblock copolymer, and Russell Hajdaj of the NIST Microfabrication Facility for his help in creating the overlay roughness sample.

REFERENCES

1. T.A. Germer, C.C. Asmail, and B.W. Scheer, "Polarization of out-of-plane scattering from microrough silicon," Opt. Lett. **22**, 1284-1286 (1997).
2. T.A. Germer, "Angular dependence and polarization of out-of-plane optical scattering from particulate contamination, subsurface defects, and surface microroughness," Appl. Opt. **36**, 8798-8805 (1997).
3. T.A. Germer and C.C. Asmail, "Polarization of light scattered by microrough surfaces and subsurface defects," J. Opt. Soc. Am. A **16**, 1326-1332 (1999).
4. L. Sung, G.W. Mulholland, and T.A. Germer, "Polarized light-scattering measurements of dielectric spheres upon a silicon surface," Opt. Lett. **24**, 866-868 (1999).
5. E. Kröger and E. Kretschmann, "Scattering of light by slightly rough surfaces or thin films including plasma resonance emission," Z. Physik **237**, 1-15 (1970).
6. J.C. Stover, *Optical Scattering: Measurement and Analysis*, (SPIE Optical Engineering Press, Bellingham, WA, 1995).
7. T.A. Germer and C.C. Asmail, "Microroughness-blind optical scattering instrument," United States Patent 6,034,776 (2000).
8. F.E. Nicodemus, J.C. Richmond, J.J. Hsia, I.W. Ginsberg, and T. Limperis, *Geometrical Considerations and Nomenclature for Reflectance*, (National Bureau of Standards, Gaithersburg, 1977).
9. H.C. van de Hulst, *Light Scattering by Small Particles*, (Dover, New York, 1981).
10. C.F. Bohren and D.R. Huffman, *Absorption and Scattering of Light by Small Particles*, (Wiley, New York, 1983).

11. D.S. Flynn and C. Alexander, “Polarized surface scattering expressed in terms of a bidirectional reflectance distribution function matrix,” Opt. Eng. **34**, 1646-1650 (1995).
12. J.M. Elson, “Multilayer-coated optics: guided-wave coupling and scattering by means of interface random roughness,” J. Opt. Soc. Am. A **12**, 729-742 (1995).
13. J.M. Elson, J.P. Rahn, and J.M. Bennett, “Light scattering from multilayer optics: comparison of theory and experiment,” Appl. Opt. **19**, 669-679 (1980).
14. J.M. Elson, “Diffraction and diffuse scattering from dielectric multilayers,” J. Opt. Soc. Am. **69**, 48-54 (1979).
15. J.M. Elson, “Infrared light scattering from surfaces covered with multiple dielectric overlayers,” Appl. Opt. **16**, 2872-2881 (1977).
16. J.M. Elson, “Light scattering from surfaces with a single dielectric overlayer,” J. Opt. Soc. Am. **66**, 682-694 (1976).
17. T.A. Germer, *SCATMECH: Polarized Light Scattering C++ Class Library*, http://physics.nist.gov/scatmech.
18. T.A. Germer and C.C. Asmail, “Goniometric optical scatter instrument for out-of-plane ellipsometry measurements,” Rev. Sci. Instr. **70**, 3688-3695 (1999).
19. T.A. Germer and C.C. Asmail, “A goniometric optical scatter instrument for bidirectional reflectance distribution function measurements with out -of-plane and polarimetry capabilities,” in *Scattering and Surface Roughness*, Z.-H. Gu and A.A. Maradudin, Eds., Proc. SPIE **3141**, 220-231, (1997).
20. B.W. Scheer, “Development of a physical haze and microroughness standard,” in *Flatness, Roughness, and Discrete Defect Characterization for Computer Disks, Wafers, and Flat Panel Displays*, J.C. Stover, Ed., Proc. SPIE **2862**, 78-95, (1996).
21. T.A. Germer, “Measurement of roughness of two interfaces of a dielectric film by scattering ellipsometry,” Phys. Rev. Lett. **85**, 349-352 (2000).
22. M.J. Fasolka and A.M. Mayes, “Block copolymer thin films: Physics and applications,” Ann. Rev. Mater. Res. **31**, 323-355 (2001).
23. M.J. Fasolka, T.A. Germer, and A. Karim, in preparation (2003).